Initial mechanisms for the decomposition of electronically excited energetic materials: $_{1,5'}$–BT, $_{5,5'}$–BT, and AzTT

Bing Yuan, Zijun Yu, and Elliot R. Bernstein

Citation: The Journal of Chemical Physics **142**, 124315 (2015); doi: 10.1063/1.4916111
View online: http://dx.doi.org/10.1063/1.4916111
View Table of Contents: http://aip.scitation.org/toc/jcp/142/12
Published by the American Institute of Physics

Initial mechanisms for the decomposition of electronically excited energetic materials: 1,5′-BT, 5,5′-BT, and AzTT

Bing Yuan, Zijun Yu, and Elliot R. Bernstein[a)]
Department of Chemistry, Colorado State University, Fort Collins, Colorado 80523-1872, USA

(Received 27 January 2015; accepted 12 March 2015; published online 31 March 2015)

Decomposition of nitrogen-rich energetic materials 1,5′-BT, 5,5′-BT, and AzTT (1,5′-Bistetrazole, 5,5′-Bistetrazole, and 5-(5-azido-(1 or 4)H-1,2,4-triazol-3-yl)tetrazole, respectively), following electronic state excitation, is investigated both experimentally and theoretically. The N_2 molecule is observed as an initial decomposition product from the three materials, subsequent to UV excitation, with a cold rotational temperature (<30 K). Initial decomposition mechanisms for these three electronically excited materials are explored at the complete active space self-consistent field (CASSCF) level. Potential energy surface calculations at the CASSCF(12,8)/6-31G(d) level illustrate that conical intersections play an essential role in the decomposition mechanism. Electronically excited S_1 molecules can non-adiabatically relax to their ground electronic states through $(S_1/S_0)_{CI}$ conical intersections. 1,5′-BT and 5,5′-BT materials have several $(S_1/S_0)_{CI}$ conical intersections between S_1 and S_0 states, related to different tetrazole ring opening positions, all of which lead to N_2 product formation. The N_2 product for AzTT is formed primarily by N–N bond rupture of the $–N_3$ group. The observed rotational energy distributions for the N_2 products are consistent with the final structures of the respective transition states for each molecule on its S_0 potential energy surface. The theoretically derived vibrational temperature of the N_2 product is high, which is similar to that found for energetic salts and molecules studied previously. © *2015 AIP Publishing LLC.* [http://dx.doi.org/10.1063/1.4916111]

I. INTRODUCTION

The search for new energetic materials is focused on a number of requirements: (1) high energetic performance; (2) substantial thermal stability; (3) low sensitivity to initiation; and (4) low toxicity, especially toward aquatic organisms and humans.[1–4] Research on nitrogen rich energetic materials is pursued in many research groups worldwide. The energy of nitrogen rich compounds is derived from their high positive heats of formation, which is directly attributable to the large number of inherently energetic C—N and N—N bonds, rather than from combustion of a carbon backbone or ring/cage strain, as often suggested for TNT, HMX, RDX, and CL-20.[4–6] This shows that high nitrogen content compounds could ideally store a large amount of energy. Moreover, nitrogen rich compounds have favorable insensitivity, good explosive performance, as well as generation of N_2 molecules as an end product of propulsion or explosion reactions, which effectively avoids environmental pollution and health risks.[4,7]

Nitrogen rich, N-heterocyclic ligands, such as triazoles and tetrazoles (see Figure 1), play an important role in the design of new energetic compounds.[6–9] The most promising N-heterocyclic backbone for the preparation of high performance energetic materials is considered to be the tetrazole ring. Tetrazole is an azo compound with high nitrogen content (~60 atom %), inherently energetic N–N and N–C bonds, high aromatic ring strain, and high crystal density: these properties have enabled the preparation of a variety of high performance primary and secondary explosives.[4,6–8]

In recent years, synthesis of two linked azoles (furazan, 1,2,4-triazole, tetrazole, etc.) for energetic molecules has been a focus of several research groups. The initial major decomposition product of these molecules is N_2, featuring the highly stable N–N triple bond instead of the less stable double and single bonds of the azoles.[7] Heterocycles connected by C–C bond, such as bistriazoles and bistetrazoles, have been shown to possess the desired combination of stability, energy storage, and energy release properties.[4,8,9] The synthesis of 5,5′-bistetrazole was reported in 1914 and it can be obtained in good yield and high purity from the reaction of sodium azide, sodium cyanide, and manganese dioxide in water.[7,11] 5,5′-bistetrazole and its derivatives have been intensely studied regarding their energetic properties: this interest has resulted in a wide variety of applications.[5,7,10,11] Löbbecke *et al.* pointed out that 5,5′-bistetrazole has better overall energetic performance than a single tetrazole.[8] The 1,5′-bistetrazole dates back to 1985,[7] but its energetic applications were much more recently investigated, mostly with regard to gas generation, owing to its high nitrogen content; nonetheless, the decomposition mechanisms for 5,5′-bistetrazole and its isomer 1,5′-bistetrazole remain largely unexplored.[7] Besides bistetrazole compounds, the combination of two different heterocycles is advantageous due to the vast possibilities for tailoring energetic behavior and performance. The C–C combination of 1,2,4-triazoles with a tetrazole moiety benefits from higher energy content of the tetrazole ring, higher stability of the triazole ring, and the potential for substitution

a)Author to whom correspondence should be addressed. Electronic mail: erb@lamar.Colostate.edu

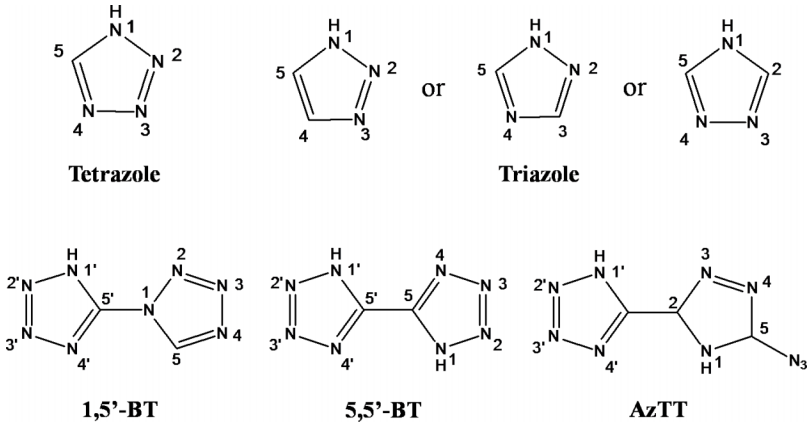

FIG. 1. Chemical structures of tetrazole, triazole, 1,5′-BT, 5,5′-BT and AzTT with atoms numbered for the rings.

at the second carbon atom of the triazole ring with various energetic groups, such as, N_3, NO_2, or NH_2.[6,12]

In this study, we focus on understanding the first step in the unimolecular decomposition mechanisms, initiated by electronic excitation, for three high nitrogen content energetic materials: 5,5′-bistetrazole (5,5′-BT), 1,5′-bistetrazole (1,5′-BT), and 5-(5-azido-(1or 4)H-1,2,4-triazol-3-yl)tetrazole (AzTT). The structures of these three energetic materials are shown in Figure 1. The overall decomposition process following electronic excitation implies that energetic materials are excited to high energy electronic states via sparks, arcs, pressure waves, photons, etc., to initiate release of their stored energy.[13–15] Following excitation to S_n they rapidly return to the ground electronic state S_0 with all the acquired excitation energy now placed in the vibrational degrees of freedom of S_0, enabling rapid and energetic breaking of bonds and generation of hot small radicals and molecules. The further reactions, called the secondary chemistry, are reactions between vibrationally hot small molecules and radicals and neighboring energetic molecules from the first decomposition step. This mechanism for the release of stored energy from energetic molecules has been previously discussed in the literature since the early 1970s.[16,17]

Comparison of the energetic properties and detonation parameters of these three energetic materials and the older energetic materials (e.g., RDX HMX, and CL-20) is discussed by other researchers: compared to RDX, these three high nitrogen content energetic materials have higher impact sensitivity and friction sensitivity, their enthalpy and energy of formation are ten times higher than those of RDX, and their energy of explosion is about two-thirds of that of RDX.[7,8,12] Although 1,5′-BT, 5,5′-BT, and AzTT do not perform as well as RDX with regard to energy of explosion,[7,8,12] they are less toxic. Since tetrazole and triazole rings are currently common molecules for creating new energetic materials with low sensitivity and high energy performance, their unimolecular decomposition mechanisms are important to investigate.

Similar to our previous work, we focus on the decomposition of isolated energetic materials experimentally, and calculate the decomposition mechanism of single energetic molecules theoretically. Based on the phenomenon of triboluminescence found for many organic and inorganic compounds, “low energy” pressure waves (for example, gentle, hand grinding) in crystals generate excited electronic states, for many atoms, molecules, ions, and radicals. Parent molecule emission (i.e., classical triboluminescence) can be quenched as electronic energy evolves to vibrational energy, through ultrafast, non-adiabatic, and conical intersections (e.g., S_n–S_0). This phenomenon, in a condensed phase or an isolated molecule, occurs to generate dominant local ultrafast molecular kinetics even in the presence of relatively strong van der Waals (e.g., hydrogen bonding, ca. 40 kJ/mol) condensed phase interactions, because intramolecular vibrational coupling is larger than intermolecular molecule-phonon coupling.[18] Thereby, the isolated molecule experiments and theory represent a reasonable approximation to the primary, initial behavior for the decomposition of energetic molecules in general condensed phase materials. In this case, conical intersections, which are the crossing and interaction point between two electronic states, play a key role in the ultrafast (~100 fs) decomposition pathways.[19–23] The presented discussion includes product energy distribution, at the initial ultrafast molecular level, following electronic excitation for the isolated energetic material molecules of interest. Determination of reaction (decomposition and stored energy release) mechanisms, kinetics, and dynamics for these large energetic molecules energized to excited electronic states emphasizes the importance of fundamental chemical physics to the technological advance of newly synthesized energetic materials, energy storage systems, and fuels.

In sum, in our experimental study, energy resolved spectra of the initial product molecule N_2 are studied to define the initial decomposition dynamics of the energetic material isolated molecule through elucidating the rotational temperature of the N_2 product. Potential energy surfaces for the excited and ground electronic states are explored theoretically employing quantum chemistry calculations (Gaussian 09, complete active space self-consistent field (CASSCF)). The detailed decomposition mechanisms of 1,5′-BT, 5,5′-BT, and AzTT energetic materials are thereby determined and discussed. As none of these energetic species contains an NO_2 group, ring opening decomposition mechanisms are proposed. The decomposition mechanisms for high nitrogen content energetic materials with and without an azide group are compared. A detailed explication of the decomposition mechanisms for these energetic species is provided which

generates insights into the behavior of bistetrazoles and mixed tetrazoles/triazoles as energetic materials. These studies are both fundamental and practical as they make advances toward the application of fundamental chemical physics specifically to the behavior of new organic, energy storage materials. Additionally, this strategy generates a new, applications oriented approach for explication of energetic species, and their fundamental behavior and properties as energy storage systems.

II. EXPERIMENTAL PROCEDURES

The experimental setup consists of a matrix-assisted laser desorption (MALD) system, a supersonic jet expansion nozzle, and a time of flight mass spectrometer (TOFMS). Details of the instrumental design are described in our previous papers.[22,23] The nozzle used for the molecular beam generation is constructed from a Jordan Co. pulsed valve and a laser ablation attachment. The laser desorption head is attached to the front of the pulsed valve with three significant parts: (1) a 2×60 mm channel for the expansion gas from the nozzle, (2) a conical channel (3 mm at the outside and 1 mm at the intersection with gas expansion channel) for the ablation laser beam perpendicular to the expansion gas channel, and (3) a 40 mm diameter hole for the sample drum. The sample drum fits into the 40 mm hole and is simultaneously rotated and translated by a motor and gear system in the vacuum in order to present a fresh sample region to the ablation laser for each pulse. The nonvolatile samples are desorbed from the drum by 532 nm ablation laser, entrained in the flow of He carrier gas under a pressure of 80 psi through the 2×60 mm channel in the laser desorption head and expanded into the vacuum chamber. With 80 psi He backing pressure for the closed pulsed valve, the chamber pressure remains 8×10^{-8} torr; with the valve open at 10 Hz, the chamber pressure increases to 4×10^{-7} torr.

All sample drums for MALD are prepared by wrapping a piece of porous filter paper around a clean Al drum. A solution of 0.02 mol/l matrix (Rhodamine6G) and 0.02 mol/l sample in water is uniformly sprayed on the drum surface while it is rotating under a halogen heat lamp in a fume hood to make sure the sample coating is dry. An air atomizing spray nozzle (Spraying System Co.) with siphon pressure of 10 psi is used to deposit sample plus matrix on the filter paper surface. The dried drum with well-distributed sample is then placed in the laser ablation head assembly and put into the vacuum chamber for decomposition reaction studies. All three samples are supplied by Professor Thomas M. Klapökte, Ludwig-Maximilian University of Munich.

In addition to the ablation laser, one or two other lasers are required to photo-excite the sample in the beam and then detect the dissociated fragments. Laser ablation of any molecule will generate both ionic and neutral species. In our apparatus, only the neutrals can enter the electric field extraction/ionization region because the plates are continuously charged to 4.0 kV and 3.75 kV, as is usual for a linear 1 min time of flight mass spectrometer with a 3 plate ion focusing region for laser ionization of neutrals. Negative ions entering this region are attracted to the high voltage plate and are not deflected toward the flight tube/detector, and positive ions undergo a curved deflection as they enter the high voltage field region and do not reach the microchannel detector at all or are dispersed by the field to generate only a background signal, which is known to be quite small (<1 mV) by measurement.

A single pump/probe laser is used at 283 nm for sample initiation and N_2 detection following a one color (2 + 2) resonance-enhanced four photon ionization (REMPI) scheme [$a^1\Pi_g(v' = 1) \leftarrow X^1\Sigma_g(v'' = 0)$ and $I \leftarrow a$ transitions] through TOFMS.[24–26] The UV laser wavelengths for this process are generated by a dye laser, pumped by the second harmonic (532 nm) of an Nd: yttrium aluminum garnet laser's fundamental output (1.064 μm), in conjunction with a frequency doubling system. As four photons are required in one detection, the typical pulse energy of the UV laser is about 6-7 mJ/pulse, giving an intensity of $\sim 2.4 \times 10^9$-2.8×10^9 W/cm^2 for a 8 ns pulse duration. The molecular beam is perpendicularly crossed by the UV laser beam, which is focused to a spot size of about 0.2 mm diameter at the ionization region of the TOFMS. Before the detection of energetic materials, a 3% N_2 in He gas mixture is prepared and studied for the calibration of N_2 rotational spectrum.

The timing sequence of pulsed nozzle, ablation laser, and excitation/ionization laser is controlled by time delay generators (SRS DG535). The experiment is run at a repetition rate of 10 Hz. Ion signals in the TOFMS are detected by a microchannel plate (MCP), and signals are recorded and processed on a personal computer (PC) using an ADC card (Analog Devices RTI-800) and a boxcar averager (SRS SR 250).

Since no experimental data exist for vertical excitation energies of 1,5′-BT, 5,5′-BT, and AzTT molecules, in order to determine the accuracy of theoretical calculation for the higher electronic states, the experimental UV-vis absorption spectra of these three energetic materials are taken with an UV-vis-near infra-red Varian Cary 500 spectrometer. The three samples are dissolved in water with concentrations between 10^{-6} and 10^{-5} mol/l. These spectra are discussed in Sec. IV.

III. COMPUTATIONAL METHODS

Most calculations are executed at the CASSCF(12,8)/6-31G(d) level of theory within the Gaussian 09 program. To explore the excited state potential energy surfaces, the active space comprises 12 electrons distributed in 8 orbitals, denoted as CASSCF (12,8). No symmetry restrictions are applied for the calculations. For the calculation of all three energetic materials, equilibrium geometry calculations are conducted taking the total charge as neutral and the spin multiplicity as 1 (S = 0). Orbitals used for the 1,5′-BT active space are two π-bonding orbitals around each tetrazole ring $\pi_{1,\mathrm{ring}}$ and $\pi_{2,\mathrm{ring}}$, four σ-nonbonding orbitals around the whole molecular system $n\sigma_1$, $n\sigma_2$, $n\sigma_3$, and $n\sigma_4$, and two π-antibonding orbitals around the whole molecular system π_1^* and π_2^* as shown in Figure 2(a). Orbitals used for the 5,5′-BT active space are similar as 1,5′-BT. Orbitals used for the AzTT active space are shown in Figure 2(b). They include three π-nonbonding orbitals around the triazole or tetrazole ring $\pi_{\mathrm{ring},1}$, $\pi_{\mathrm{ring},2}$

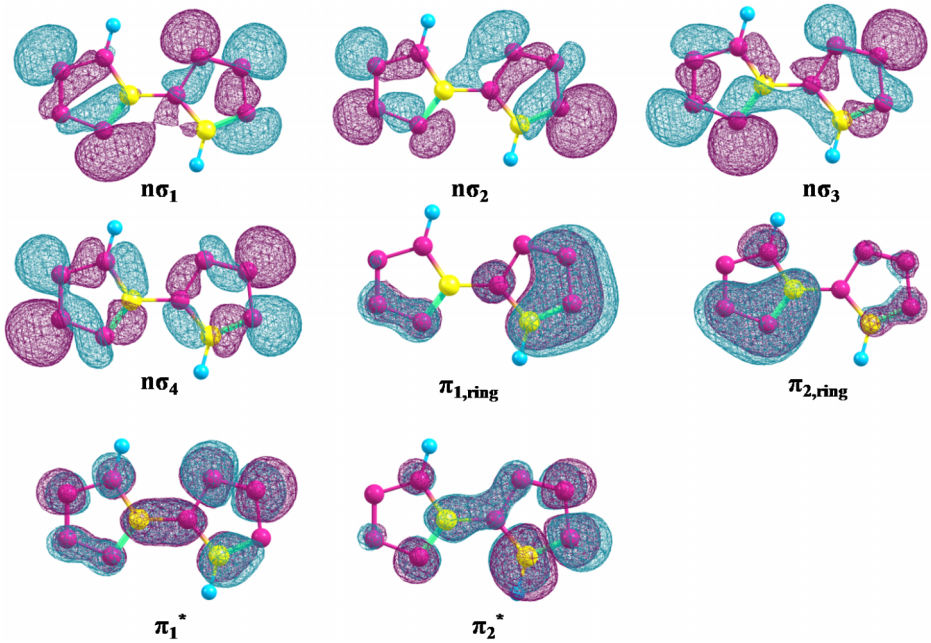

(a)

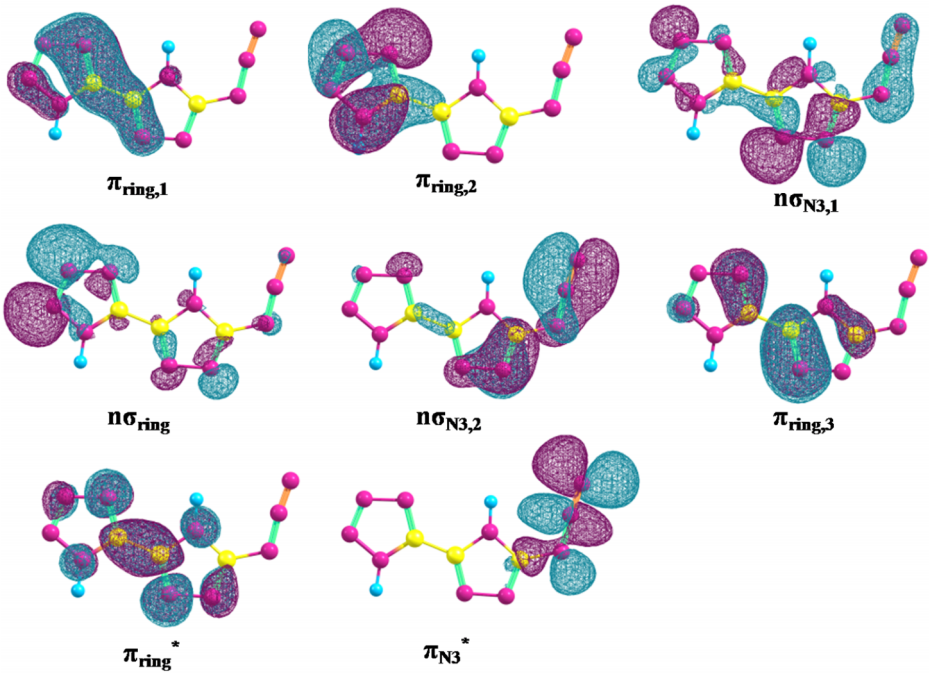

(b)

FIG. 2. (a) Orbitals used in the active space of CASSCF calculations for 1,5′-BT. The (12,8) active space comprises two π-bonding orbitals ($\pi_{1,\mathrm{ring}}$ and $\pi_{2,\mathrm{ring}}$), four σ-nonbonding orbitals ($n\sigma_1$, $n\sigma_2$, $n\sigma_3$, and $n\sigma_4$), and two π-antibonding orbitals (π_1^* and π_2^*). For atoms in the structure, yellow is carbon, pink is nitrogen, and blue is hydrogen. (b) Orbitals used in the active space of CASSCF calculations for AzTT. The (12,8) active space comprises three π-nonbonding orbitals ($\pi_{\mathrm{ring},1}$, $\pi_{\mathrm{ring},2}$, and $\pi_{\mathrm{ring},3}$), one σ-nonbonding orbital $n\sigma_{\mathrm{ring}}$, two σ-nonbonding orbitals ($n\sigma_{N3,1}$ and $n\sigma_{N3,2}$), two π-antibonding orbitals (π_{ring}^* and π_{N3}^*). For atoms in the structure, yellow is carbon, pink is nitrogen, and blue is hydrogen.

and $\pi_{\mathrm{ring},3}$, one σ-nonbonding orbital on both the triazole and tetrazole rings $n\sigma_{\mathrm{ring}}$, two σ-nonbonding orbitals on the azide group $n\sigma_{N3,1}$ and $n\sigma_{N3,2}$, one π-antibonding orbital around the triazole and tetrazole ring π_{ring}^*, and one π-antibonding orbital around the azide group π_{N3}^*. For 1,5-BT and 5,5-BT, the decomposition path is a tetrazole ring opening channel; thus, both non-bonging orbitals and π orbitals around the tetrazole ring are chosen for the reaction description. For AzTT, the decomposition reactions contain the $-N_3$ group breaking and tetrazole/triazole ring opening; thus, orbitals around both the N_3 group and azole rings are selected. Chosen orbitals are the HOMO/LUMO orbitals and orbitals close in energy to the HOMO and LUMO. Eight orbitals are selected because this is maximum limit for CASSCF for conical section calculations due to the need for analytic second derivatives. The agreement between theory and experiment demonstrates that 8 orbitals are sufficient in this instance.

Excitation energies are calculated by state averaging over the ground and excited states with equal weights for each state. Larger basis sets than 6-31g(d) for CASSCF calculations do

not substantially improve the results and understanding of the reaction mechanisms.[27]

Critical points (minima and transition state structures) are characterized by analytical frequency calculations, and minimum energy paths are calculated using an intrinsic reaction coordinate (IRC) algorithm implemented in the Gaussian 09 program suite. To find the transition and intermediate states along the reaction pathways, a relaxed scan optimization algorithm as implemented is employed in which all geometrical parameters except for the specified bond distance are optimized and electronic energies are monitored as the specified bond is elongated. This scan uses the key word "opt = modredundant." The bond length increase for each step is 0.1 Å for a total scan length of 2.5 Å. In the scan, the structure with peak potential energy is most likely a transition state, and the structure with potential energy in a valley is most likely an intermediate state. To verify this conclusion and obtain a more accurate potential energy surface for the transition/intermediate states, the molecular structure provided in the scan is used as the initial structure in the following optimization calculation with CASSCF(12,8) as the active space. For all three energetic materials, the transition state on the first excited state cannot be converged using the CASSCF calculation. Therefore, a TD-DFT/6-31g(d) method is applied to find the excited transition state. The transition state energy on the excited electronic state is calculated using the energy difference between the excited transition point from a TD-DFT calculation and the Franck Condon structure on the ground electronic state also from a DFT calculation. The accuracies of the calculations along the reaction pathway are difficult to estimate since experimental information about the conical intersections and the transition states is not available. Calculations presented in this paper, however, are based on the experimental observations including decomposition product N_2 and the internal energy distributions within this product. Therefore, the proposed reaction pathways based on the computational results provide a reasonable, and at minimum qualitative, interpretation for the experimental observations.

IV. EXPERIMENTAL RESULTS AND DISCUSSION

A. UV-vis absorption spectra of 1,5′-BT, 5,5′-BT, and AzTT

The UV-vis absorption spectra of 1,5′-BT, 5,5′-BT, and AzTT are shown in Figure 3: the maximum absorption wavelengths for these three energetic materials are 221, 220, and 234 nm, respectively. For N_2 product decomposition, the laser wavelength is 283 nm, which is lower in energy than the absorption maximum; therefore, the excitation and decomposition of these three energetic materials occur through a two photon absorption. As N_2 detection is a one color, (2 + 2), REMPI process, the laser energy/pulse is ca. 10 times greater than that employed for (1 + 1) REMPI detection, such as employed for NO. The overall excitation/N_2 detection process for 1,5′-BT, 5,5′-BT, and AzTT is thereby a six photon process: this can be compared to the excitation/NO detection process for nitramines, which is a three photon process overall.

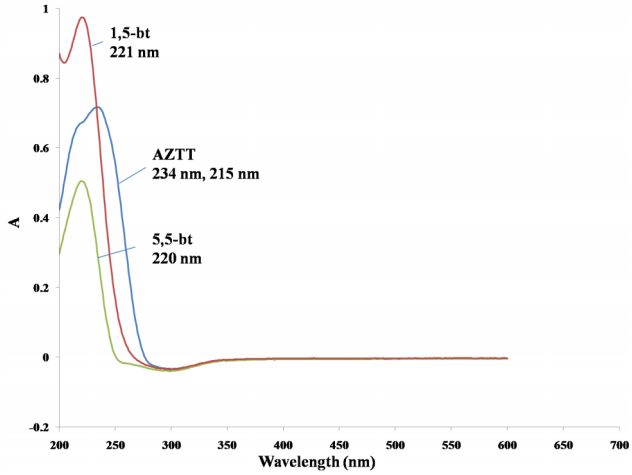

FIG. 3. UV-vis absorption spectra of 1,5′-BT, 5,5′-BT, and AzTT with maximum absorption wavelengths. All three samples are dissolved in distilled water.

B. Decomposition product N_2

Decomposition product N_2 is observed from electronically excited 1,5′-BT, 5,5′-BT, and AzTT employing 283 nm excitation and TOFMS detection. The 283 nm excitation wavelength corresponds to the resonance (1-0) vibronic band of the $a^1\Pi_g \leftarrow X^1\Sigma_g$ electronic transition of the N_2 product. REMPI (2 + 2) rotationally resolved spectra of the N_2 product from these three energetic materials are obtained by scanning the laser excitation wavelength. The line width of the N_2 mass peak is 10 ns (the laser pulse width) and laser beam intensity is varied without change in the N_2 TOFMS line width. Excited electronic states of these three energetic materials, which might be generated in the ablation process, are effectively relaxed and cooled in the highly collisional expansion process, through the supersonic nozzle. Additionally, the 532 nm ablation laser is not directly resonant for these molecules and these photons are almost completely absorbed by the R6G matrix. The arrival time at the ionization/extraction region of the TOFMS for the species generating the N_2 spectrum is consistent with that of a large mass molecule (ca. 300–350 amu).

Figure 4 shows the spectra of $a^1\Pi_g(v' = 1) \leftarrow X^1\Sigma_g(v'' = 0)$ rovibronic transition of the N_2 molecule arising from a 3% N_2/He mixture, 1,5′-BT, 5,5′-BT, and AzTT following excitation to their excited electronic states. The rotational spectra of N_2 from the N_2 gas mixture and the three energetic materials have similar patterns: the most intense peak in each spectrum of N_2 corresponds to the S_0 peak in the S branch rotational transitions. Other peaks, including S_1 and S_2 in the S branch, Q_1 peak in the Q branch, and P_2 in the P branch rotational transitions, are labeled in Figure 4.[25,26] The rotational spectrum for the N_2/He mixture expansion is similar to that of the previous studies,[28] indicating a rotational temperature of about 20 K. Details of this calculation are published in a previous paper.[29]

The N_2 signals from energetic materials are much less intense than those of the N_2 gas mixture, as only the S_0 peak can be consistently observed in the rotational spectra. Therefore, through comparison to the spectrum of the N_2 gas

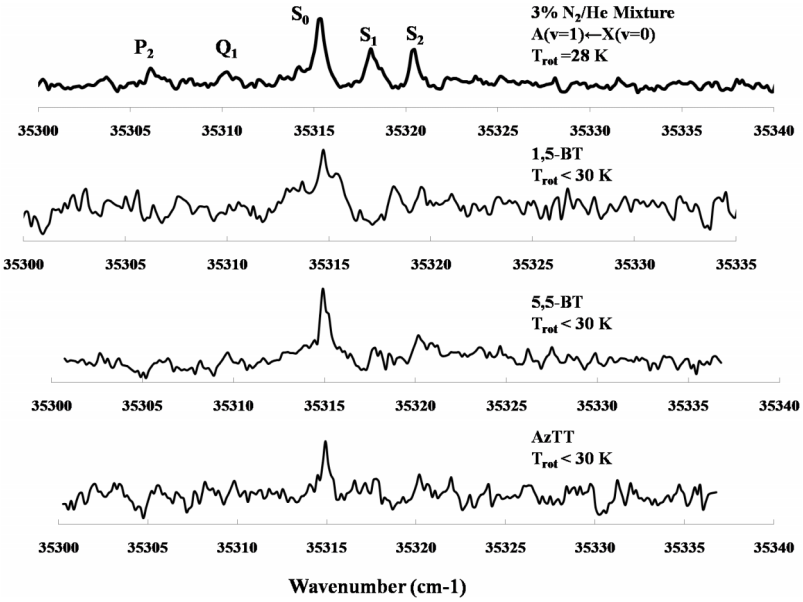

FIG. 4. One color (2+2) REMPI spectra of the vibronic transitions $a^1\Pi_g(v'=1) \leftarrow X^1\Sigma_g(v''=0)$ of N_2 from 3% N_2/He mixture, and from electronic state excitation of 1,5′-BT, 5,5′-BT, and AzTT. The rotational temperature of the 3% N_2 mixture calculated from a Boltzmann plot equals 28 K. The rotational temperatures of N_2 decomposition products from 1,5′-BT, 5,5′-BT, and AzTT (as indicated) are estimated to be smaller than 30 K.

mixture and the previous studies, the rotational temperatures of the N_2 product released from all three energetic materials are assigned only as lower than 30 K. This result is similar to that for the high N content energetic salts.[29]

To find the vibrational temperature of the N_2 product, the rotational spectra of N_2 should be obtained for several vibronic bands. The signal intensity of the reported N_2 rotational transition from ground rovibronic state $v'' = 0$ is ca. 80 mV, about 4 times higher than the noise level. To get N_2 rovibronic transition spectra starting from $v'' \geqslant 1$ of the ground electronic state, the signal intensity should be 5-10 times lower than the above 80 mV, assuming an established vibrational temperature. This estimated transition intensity is under the detection limit for the measurement. Consequently, further N_2 rovibronic bands were not obtained in these experiments, and thus, vibrational temperature cannot be determined for the N_2 products of these molecules.

TOF mass spectra, obtained under 283 nm excitation employed especially for N_2 detection, display a few very weak additional features in the low mass region. Compared to the N_2 signal, however, these features are much weaker, and their intensity remains constant as the excitation wavelength is scanned. These additional weak features are most likely not a result of a major decomposition pathway from any of the energetic molecules.

V. THEORETICAL RESULTS AND DISCUSSION

Experimental results yield that N_2 molecules are initial nanosecond electronic excitation decomposition product for the energetic systems explored under this study. In order to understand the experimental data more completely and derive reaction mechanisms, theoretical calculations of molecular geometries and energies for the Franck-Condon structure, conical intersections, transition states, and intermediate states along both the ground and excited states potential energy surfaces are performed for the three energetic materials. The calculational algorithm employed for these studies reproduces the experimental observations with regard to product generation and energy distribution for each product molecule. This is all one can require of a chosen calculational method: the calculations predict or generate the observed behavior. The approach to calculation of the reaction mechanism (based on the above presented algorithm and approximations) is justified, thereby, by the results of the calculations with regard to product molecules, their energy dynamics and distributions, and the overall reaction kinetics. The theoretical reaction paths with potential energies and molecular geometries are shown in Figs. 5-10.

Nine possible decomposition mechanisms are explored for 1,5′-BT in the theoretical study, through nine different conical intersections between the S_1 and S_0 electronic states, which are related to eight different tetrazole ring opening positions (i.e., seven different reaction coordinates or slices through the multi dimensional potential energy surfaces (PESs)) plus a non-ring opening one. Similarly, five possible decomposition mechanisms are explored for 5,5′-BT, including four different conical intersections between the S_1 and S_0 states for four different tetrazole ring opening positions and a non-ring opening one. As 5,5′-BT has a symmetric structure, the different ring opening positions are lower in energy than those for 1,5′-BT. Totally eight possible decomposition mechanisms are considered for AzTT, through six different triazole and tetrazole ring opening positions, as well as reactions for its azide group. All these reaction channels are chosen because they are energy available and accessible for the creation of N_2 products. The actual reaction pathways used by these molecules will depend on different factors, for example, the rate of internal vibrational energy redistribution, the heights of reaction barriers, and the rate of non-adiabatic transition through the different conical intersections, which can only be assessed by theoretical calculations.

Calculations at the CASSCF(12,8)/6-31G(d) theoretical level are employed to determine the vertical excitation energies for 1,5′-BT, 5,5′-BT, and AzTT from the ground electronic state S_0 (Franck Condon (FC) structure) to the first excited

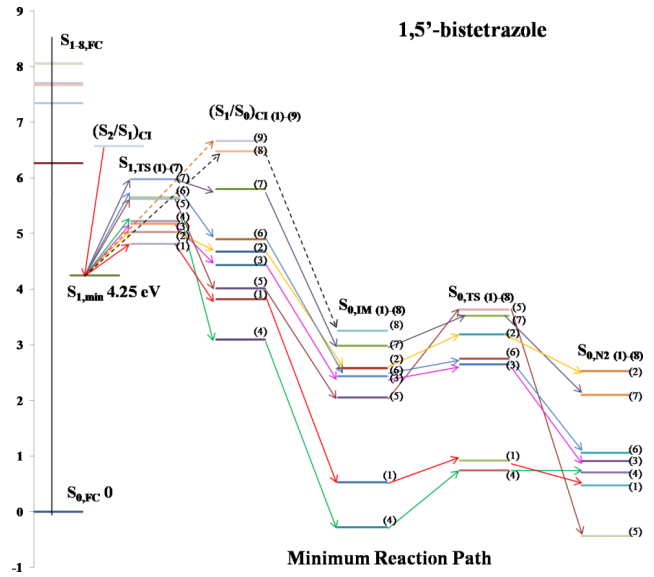

FIG. 5. A schematic one-dimensional projection of the multi-dimensional energy surfaces for nine 1,5′-BT dissociation paths computed at the CASSCF(12,8)/6-31G(d) level of theory. These nine reaction paths contain eight tetrazole ring opening channels and one non-ring opening channel. The red, orange, violet, green, brown, blue, purple, black, and yellowish brown arrows represent (1)–(9) different reaction channels for N_2 dissociation, respectively. $S_{0,FC}$ is the optimized minimum energy of 1,5′-BT on the S_0 state with a planar structure. $(S_1/S_0)_{CI(1)\text{-}(9)}$ are the conical intersections between the S_0 and S_1 states, and (1)-(9) are related to different tetrazole ring opening positions (reactions, minimum energy coordinates) in different reaction channels. $S_{1,TS(1)\text{-}(7)}$ are the excited transition states on the S_1 electronic state surface between the minimum structure $S_{1,min}$ on S_1 and their related conical intersections. $S_{0,IM(1)\text{–}(8)}$ are the intermediate states on the ground electronic state S_0 after $(S_1/S_0)_{CI(1)}$, while $S_{0,TS(1)\text{-}(8)}$ are the transition states on the S_0 state following each intermediate state ($S_{0,IM(1)}$ to $S_{0,IM(8)}$) in the different reaction channels. $S_{0,N2(1)\text{-}(8)}$ are molecules with N_2 dissociated products on the S_0 state.

state S_1. Under the chosen experimental conditions for these studies, the molecular excitation must be a two photon process: the energetic molecules can thereby be excited to an S_n ($n \geq 8$) electronic state. They rapidly moved to the ground electronic state through conical intersections between the different electronic states. Since the exact pathways along which these molecules move from high electronic excited states to their S_1 excited states do not significantly affect the decomposition, only the S_1 excited and S_0 ground state reaction mechanisms are discussed below.

Since data are not available for vertical excitation energies of 1,5′-BT, 5,5′-BT, and AzTT molecules, experimental UV-vis absorption spectra of these three energetic molecules are obtained to determine the accuracy of the CASSCF calculations. The vertical excitations calculated through CASSCF(12,8)/6-31G(d) (12 electrons, 8 orbitals) for the first excited electronic states S_1 of 1,5′-BT, 5,5′-BT, and AzTT are 6.26, 6.24, and 6.00 eV, respectively. The maximum absorption wavelengths for 1,5′-BT, 5,5′-BT, and AzTT in UV-vis absorption shown in Figure 3 are 221 nm (5.61 eV), 220 nm (5.63 eV), and 234 nm (5.30 eV), respectively. The commonly acceptable uncertainty range for CASSCF calculations is ±0.5 eV: calculation of the relevant excited states is thus considered reasonable. Moreover, hydrogen bond formation in a water solution should red-shift the wavelength of the UV-vis absorption spectra, which might be an additional reason for the experimental excitation being lower than those found by the CASSCF calculations. The same calculation of excited state energies through CASSCF(12, 13) for 1,5-BT and AzTT yields the S_1 state energies 6.0 and 4.81 eV, respectively. Therefore, although a CASSCF(12, 8) calculation is not a perfect theoretical approach, it is certainly sufficient for the

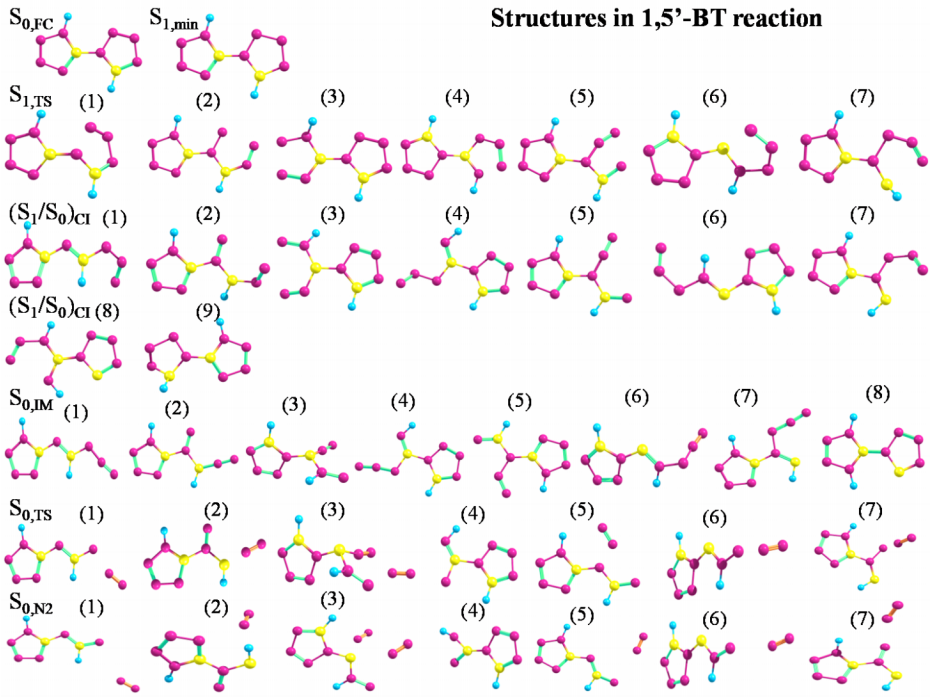

FIG. 6. Structures of all critical points and conical intersections mentioned in Figure 5 along the 1,5′-BT dissociation reaction paths (1)-(9). For atoms in the structure, yellow is carbon, pink is nitrogen, and blue is hydrogen.

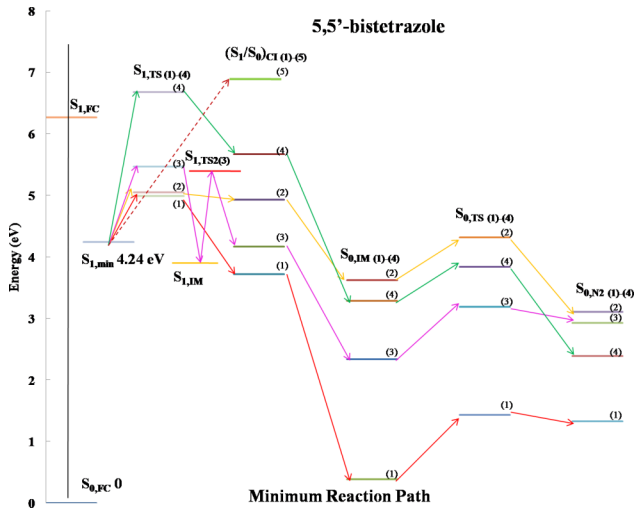

FIG. 7. A schematic one-dimensional projection of the multi-dimensional energy surfaces for five 5,5′-BT dissociation paths computed at the CASSCF(12,8)/6-31G(d) level of theory. These five reaction paths contain four tetrazole ring opening channels and one non-ring opening channel. The red, orange, violet, green, and brown arrows represent (1)–(5) different reaction channels for N_2 dissociation, respectively. $S_{0,FC}$ is the optimized minimum energy of 5,5′-BT on the S_0 state with a planar structure. $(S_1/S_0)_{CI(1)-(5)}$ are the conical intersections between the S_0 and S_1 states, and (1)-(5) related to five conical intersections in different reaction paths. $S_{1,TS(1)-(4)}$ are the excited transition states on the S_1 surface between the minimum structure $S_{1,min}$ on the S_1 excited electronic state and the related conical intersections. $S_{0,IM(1)-(4)}$ are the intermediate states on the S_0 state after $(S_1/S_0)_{CI(1)-(4)}$, while $S_{0,TS(1)-(4)}$ are the transition states on the S_0 surface following the intermediate states $S_{0,IM(1)-(4)}$ in different reaction channels. $S_{0,N2(1)-(4)}$ are N_2 dissociated products on the S_0 surface.

present mechanistic pathway and critical point identification on the S_1 and S_0 PESs for 1,5′-BT, 5,5′-BT, and AzTT.

From our previous studies, enlarging the basis set does not significantly improve the relative excitation energies or critical point energies, and therefore, a 6-31G(d) basis set is used for all calculations to maintain optimum conditions for computational cost, accuracy, and comparisons. Additionally, for the decomposition mechanisms of the three energetic materials, only molecular singlet states and singlet-singlet transitions are considered, because based on our previous femto-second studies of energetic molecules RDX and HMX, the decomposition dynamics fall into the timescale of our excitation pulse duration (ca. 100 fs).[23] These results emphasize that gas phase energetic material decomposition is an extremely fast non-adiabatic reaction at the molecular level. Molecular singlet-singlet transitions are much faster than singlet-triplet, spin forbidden transitions. The time scale of molecular fluorescence emission is between 10^{-5} and 10^{-10} s, while that for phosphorescence emission is 10^{-4} s–10 s. Therefore, singlet-triplet transitions and couplings are not the main energy conversion pathway for these energetic systems.

A. Calculations for 1,5′-BT

Schematic one-dimensional projections of the multidimensional singlet potential energy surfaces (S_0 and S_1) of 1,5′-BT, with locations and potential energies (the presented energies are not corrected for zero point energy) for different critical points and conical intersections along the minimum energy reaction paths, are plotted in Fig. 5 and the energy for each point are summarized in Table I. Figures 5 and 6 described nine different reaction channels (mechanisms) for 1,5′-BT decomposition. The reaction coordinates depicted in Figures 5 and 6 include C–N and N–N bond lengths among the tetrazole rings, either of which can be the active site for 1,5′-BT fragmentation. Arrows in Figure 5 indicate different possible reaction channels for 1,5′-BT decomposition. The structures of each critical point and conical intersection are summarized in Figure 6. In Figures 5 and 6, FC geometry $S_{0,FC}$ is the optimized minimum energy of 1,5′-BT on the

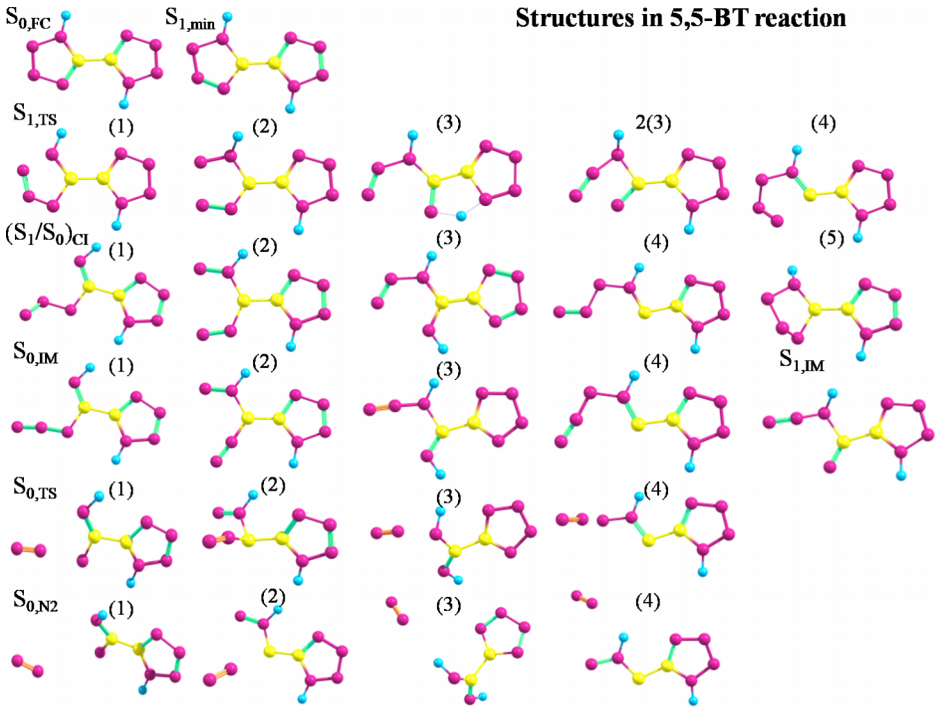

FIG. 8. Structures of all critical points and conical intersections mentioned in Figure 7 along the 5,5′-BT dissociation reaction paths (1)-(5). For atoms in the structure, yellow is carbon, violet is nitrogen, and blue is hydrogen.

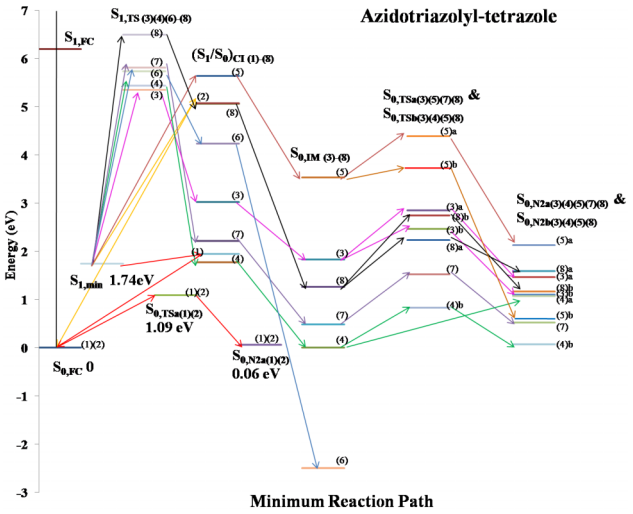

FIG. 9. A schematic one-dimensional projection of the multi-dimensional energy surfaces for eight AzTT dissociation path computed at the CASSCF(12,8)/6-31G(d) level of theory. These eight reaction paths contain six tetrazole/triazole ring opening channels and two non-ring opening channels. The red, orange, violet, green, brown, blue, purple, and black arrows represent (1)–(8) different reaction channels for N_2 dissociation, respectively. $S_{0,FC}$ is the optimized minimum energy of AzTT on the S_0 state with a planar structure. $(S_1/S_0)_{CI(1)-(8)}$ are the conical intersections between the S_0 and S_1 states, and (1)-(8) related to different ring opening positions on the tetrazole/triazole rings and rupture of the azide group in different reaction channels. $S_{1,TS(3)(4)(6)-(8)}$ are the excited transition states on the S_1 surface between the minimum structure $S_{1,min}$ and the related conical intersections. Some conical intersections do not have transition states on the S_1 state; thus, $S_{1,TS}$ is not labeled from (1) to (8). $S_{0,IM(3)-(8)}$ are the intermediate states on S_0 after $(S_1/S_0)_{CI}$, while $S_{0,TSa(3)(5)(7)(8)}$, and $S_{0,TSb(3)(4)(5)(8)}$ are the transition states on the S_0 surface following the related intermediate states $S_{0,IM(3)-(8)}$ in different reaction channels. $S_{0,N2a(3)(4)(5)(7)(8)}$ and $S_{0,N2b(3)(4)(5)(8)}$ are N_2 dissociated products on the S_0 state.

S_0 state and it is a planar structure. $(S_1/S_0)_{CI(1)-(9)}$ are the conical intersections between the S_0 and S_1 states, and (1)-(9) are related to different tetrazole ring opening positions (reactions, minimum energy coordinates) in different reaction channels. $S_{1,TS(1)-(7)}$ are the excited transition states on the S_1 electronic state surface between the minimum structure $S_{1,min}$ on S_1 state and their related conical intersections. $S_{0,IM(1)-(8)}$ are the intermediate states on the ground electronic state S_0 after $(S_1/S_0)_{CI(1)}$, while $S_{0,TS(1)-(8)}$ are the transition states on the S_0 state following each intermediate state ($S_{0,IM(1)}$ to $S_{0,IM(8)}$) in the different reaction channels. $S_{0,N2(1)-(8)}$ are molecules with N_2 dissociated products on the S_0 state.

The reaction paths in Figure 5 show that with two photon absorption, 1,5′-BT can be excited to S_n ($n > 8$), and then it moves to the first excited electronic state S_1 through several conical intersections among different electronic states. As conical intersections between high excited electronic states (S_n, $n > 2$) are typically not accurately calculated through a CASSCF algorithm, accurate energies for these conical intersections are not listed; however, the concept that molecules move from high electronic state to low electronic state through conical intersections is well documented in many studies.[19,24,26–36]

On the S_1 electronic excited state, 1,5′-BT undergoes a rapid internal conversion to the energy minimum structure $S_{1,min}$. Following this, the molecule encounters energy barriers for the transition states $S_{1,TS(1)-(7)}$ and moves to the ground electronic state through conical intersections $(S_1/S_0)_{CI(1)-(7)}$: molecules undergoing this process would place sufficient vibrational energy in the S_0 state, transferred from S_1 (and S_n) electronic energy, to dissociate. Totally seven transition states on the S_1 surface related to seven different conical intersections are identified. The energies of these transition states are listed in Table I.

The reaction path with the lowest transition state energy shown in Figure 5 is the red one (reaction path (1) in Figure 5 and Table I). Along this reaction coordinate (red path), the 1,5′-BT molecule moves from $S_{1,min}$, surmounts a 0.56 eV energy of $S_{1,TS(1)}$, and then reaches conical intersection $(S_1/S_0)_{CI(1)}$. Because the red path has the lowest energy barrier, this channel

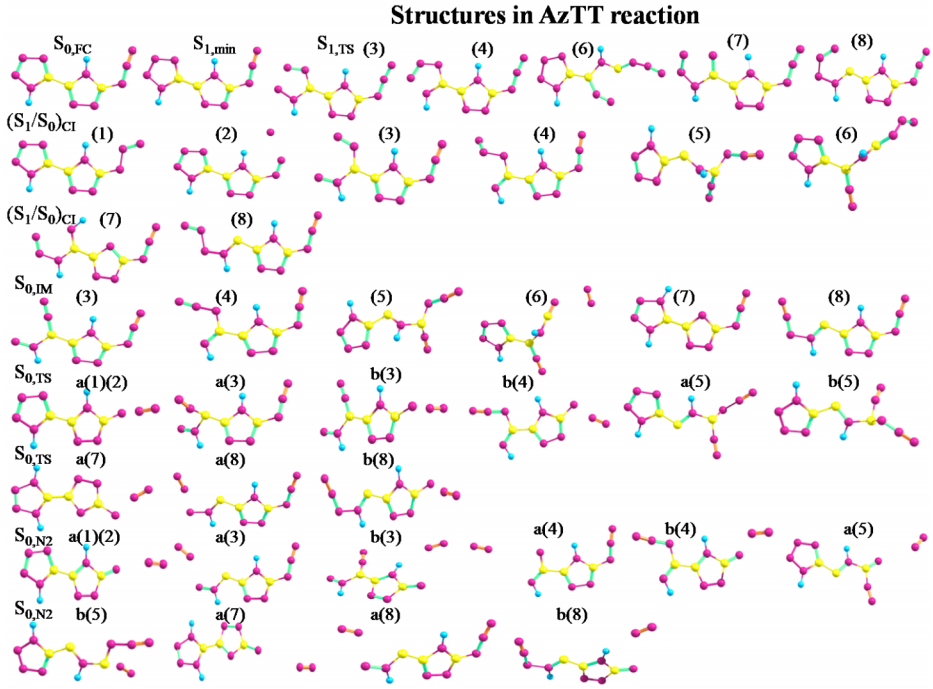

FIG. 10. Structures of all critical points and conical intersections mentioned in Figure 9 along the AzTT dissociation reaction paths (1)-(8). For atoms in the structure, yellow is carbon, pink is nitrogen, and blue is hydrogen.

TABLE I. Summary of reaction paths and critical point energies for the 1,5′-BT decomposition reaction.

Reaction path	Color	$S_{1,TS}$	$(S_1/S_0)_{CI}$	$S_{0,IM}$	$S_{0,TS}$	$S_{0,N2}$
(1)	Red	4.81	3.82	0.54	0.93	0.47
(2)	Orange	5.03	4.67	2.58	3.19	2.53
(3)	Pink	5.17	4.43	2.43	2.65	0.91
(4)	Green	5.22	3.09	−0.28	0.74	0.70
(5)	Brown	5.62	4.01	2.06	3.63	−0.44
(6)	Blue	5.65	4.90	2.57	2.75	1.06
(7)	Purple	5.98	5.80	2.98	3.52	2.10
(8)	Black	N/A	6.48	3.25	N/A	N/A
(9)	Yellowish brown	N/A	6.67	0 (back to $S_{0,FC}$)	N/A	N/A

Details of each reaction path (i)

i = 1-7	$S_{min} \rightarrow S_{1,TS(i)} \rightarrow (S_1/S_0)_{CI(i)} \rightarrow S_{0,IM(i)} \rightarrow S_{0,TS(i)} \rightarrow S_{0,N2(i)}$
i = 8	$S_{min} \rightarrow (S_1/S_0)_{CI(8)} \rightarrow S_{0,IM(8)}$
i = 9	$S_{min} \rightarrow (S_1/S_0)_{CI(9)} \rightarrow S_{0,FC}$

might be the most probable reaction path for the fragmenting system: the tetrazole ring opens at the N1–N2 bond (atoms labeled in Figure 1) along this coordinate.

The reaction path with the highest energy barrier from $S_{1,min}$ to $(S_1/S_0)_{CI(7)}$ shown in Figure 5 is the purple line (reaction path (7) in Figure 5 and Table I), which has a energy barrier of 1.73 eV through $S_{1,TS(7)}$ as the tetrazole ring opens between the C5–N4 bond. As all these energy barriers are energy available in the 2-photon absorption experimental system, all seven reaction channels are reasonable. Another two conical intersections $(S_1/S_0)_{CI(8)}$ and $(S_1/S_0)_{CI(9)}$ exist at which molecules move from $S_{1,min}$ without transition states. The energy barriers to these two conical intersections are 2.24 and 2.42 eV. The tetrazole ring at $(S_1/S_0)_{CI(8)}$ opens between N3′-N4′ and $(S_1/S_0)_{CI(9)}$ is the conical intersection between S_0 and S_1 states without a tetrazole ring opening. As $(S_1/S_0)_{CI(9)}$ has the highest energy barrier of all the conical intersections calculated for S_1/S_0, the excited 1,5′-BT molecule is most likely to finish the tetrazole ring opening process on the S_1 state PES, not on the ground electronic state S_0 PES, assuming such a distinction can be drawn at a conical intersection.

The adiabatic energy gaps between the S_1 and S_0 surfaces near conical intersections $(S_1/S_0)_{CI(1)-(9)}$ are computed to be in the range between 22 and 307 cm^{-1}, which means the S_1 and S_0 surfaces are strongly non-adiabatically coupled with one another: the small energy gap increases the probability of non-adiabatic transition from the upper to lower electronic states. As the molecule moves from the S_1 to S_0 state through $(S_1/S_0)_{CI(1)-(9)}$, the IRC algorithm shows that the steepest descent pathway for the molecule is to evolve either to a stable intermediate state $S_{0,im(1)-(8)}$ or to the Frank Condon structure $S_{0,FC}$. From the IRC scan, the tetrazole ring at $(S_1/S_0)_{CI(8)}$ closes again forming intermediate state $S_{0,IM(8)}$ and $(S_1/S_0)_{CI(9)}$ goes back to the Frank Condon structure. The tetrazole ring along these pathways should be open in order to facilitate generation of N_2 through these two conical intersections. On the other hand, the tetrazole ring remains open for intermediate states $S_{0,IM(1)-(7)}$ from $(S_1/S_0)_{CI(1)-(7)}$. From $S_{0,IM(1)-(7)}$, the molecule surmounts energy barriers in the range between 0.18 eV and 1.57 eV through the concerted transition states $S_{0,TS(1)-(8)}$ and forms the N_2 products $S_{0,N2(1)-(8)}$. N_2 products move away from the rest of the molecule or radical without obvious torque for all the reaction channels as shown in Figure 6. Therefore, N_2 products should have low rotational temperatures, as is consistent with the experimental results. The energies of the final molecule with dissociated N_2 in the seven reaction paths are in the range between −0.44 eV and 2.10 eV, which means these N_2 products should have high vibrational temperatures based on the calculations.

1,5′-BT is electronically excited in the experiment and it absorbs two laser photons for its initial excitation energy: it then decomposes initially to form N_2 products, following seven possible reaction paths as shown in Figure 5. The tetrazole ring of 1,5′-BT opens on the first excited state S_1 and the N_2 product is dissociated on the 1,5-BT ground electronic state potential energy surface. Thereby, the electronic excitation directly contributes to its ground state vibrational energy employed to break covalent chemical bonds. The energy difference between the laser energy, which is the original molecule energy, and the energy of the final structure with N_2 products and their internal energies, is the energy released from 1,5′-BT decomposition in this initial molecular decomposition step. Although we do not obtain the experimental vibrational temperature of the N_2 product, based on our theoretical calculations, N_2 should have a high vibrational temperature. This conclusion is consistent with our previous studies of energetic materials generating NO with high vibrational temperature.[22,27,29–39] With a high vibrational temperature, energy is stored in the decomposition products that can trigger secondary decomposition reactions in high density and condensed phase energetic systems.

The theoretical results demonstrate, moreover, that the decomposition dynamics are purely non-adiabatic in nature and that conical intersections can lead rapidly and efficiently to internal conversion from upper to lower electronic states through these non-adiabatic, radiationless transitions. During this internal conversion, electronic energy in the upper state is converted to vibrational energy in the lower state with a potential time scale of a few tens of femtoseconds. The molecule returns to the ground electronic potential surface far from the original FC equilibrium position, and can

thereby undergo a very different unimolecular chemistry than anticipated for its $S_{0,FC}$ structure. Conical intersections are now firmly established to be the key features in the excited electronic state chemistry of organic molecules in general, and energetic molecules in particular. From our previous studies of energetic materials with an NO_2 or N_2O_2 (nitramine) group, usually a single conical intersection is found in the reaction system, which is related to a nitro-nitrite isomeric structure.[22,27,29–39] As 1,5′-BT does not contain an NO_2 group, the tetrazole ring must open first in order to form an initial small molecule, N_2 product. Totally eight conical intersections are found on the 1,5′-BT potential surfaces between S_0 and S_1 states related to different ring opening positions in 1,5′-BT: among them, seven can lead to decomposition to an N_2 product. Given sufficient excitation energy, which position of the tetrazole ring opens first is not important, as the energy barriers for ring opening at different positions are quite close (within 1.2 eV). The tetrazole ring can open at every N–N or C–N bond to form an N_2 product with similar results.

B. Calculations for 5,5′-BT

Schematic one-dimensional projections of the multidimensional singlet potential energy surfaces (S_0 and S_1) of 5,5′-BT, with locations and potential energies (the presented energies are not corrected for zero point energy) for different critical points and conical intersections along the minimum energy reaction paths, are plotted in Figure 7, and the energy for each point is summarized in Table II. Figure 7 describes five different reaction channels for 5,5′-BT decomposition. The reaction coordinates depicted in Figure 7 include C–N and N–N bond lengths from the tetrazole ring of 5,5′-BT. Arrows in Figure 7 indicate different possible reaction channels for 5,5′-BT decomposition. The structures of each critical point and conical intersection are summarized in Figure 8. In Figures 7 and 8, FC geometry $S_{0,FC}$ is the optimized minimum energy of 5,5′-BT on the S_0 state: the structure is planar structure. $(S_1/S_0)_{CI(1)-(5)}$ are the conical intersections between the S_0 and S_1 states, and (1)-(5) related to five conical intersections in different reaction paths. $S_{1,TS(1)-(4)}$ are the transition states on the S_1 surface between the minimum structure $S_{1,min}$ on the S_1 excited electronic state and the related conical intersections. $S_{0,IM(1)-(4)}$ are the intermediate states on the S_0 surface after $(S_1/S_0)_{CI(1)-(4)}$, and $S_{0,TS(1)-(4)}$ are the transition states on the S_0 surface following the intermediate states $S_{0,IM(1)-(4)}$ in different reaction channels. $S_{0,N2(1)-(4)}$ are N_2 dissociated products on the S_0 surface.

The reaction paths in Figure 7 show that, similar to 1,5′-BT, with two photon absorption, 5,5′-BT can be excited to an S_n ($n > 8$) state, and can relax to the first excited electronic state S_1 through several conical intersections. On the S_1 state potential energy surface, 5,5′-BT undergoes a rapid internal conversion to the energy minimum structure $S_{1,min}$. The molecule surmounts the energy barrier to the transition state $S_{1,TS(1)-(4)}$, and moves to the ground electronic state surface S_0 through conical intersections $(S_1/S_0)_{CI(1)-(4)}$. Four transition states on the S_1 surface are identified for four different conical intersections $(S_1/S_0)_{CI(1)-(4)}$ and reaction coordinates. The energies of these transition states are listed in Table II. The reaction path with the lowest transition state energy shown in Figure 7 is the red path (reaction path (1) in Figure 7 and Table II). On the red path coordinate, the molecule evolves from $S_{1,min}$, surmounts a 0.75 eV energy of $S_{1,TS(1)}$ and reaches the conical intersection $(S_1/S_0)_{CI(1)}$. Due to this lowest energy barrier, the red reaction path might be the most probable one for the system: the tetrazole ring then opens at N1′-N2′ for this channel.

From $S_{1,min}$ to $(S_1/S_0)_{CI(3)}$, the purple reaction path (reaction path (3) in Figure 7 and Table II), two transition states, $S_{1,TS(3)}$ for tetrazole ring opening at N3′-N4′, and $S_{1,TS(3),2}$ for hydrogen transfer from N4′ to N1 are accessible. The energy barriers along the reaction paths from $S_{1,min}$ to $(S_1/S_0)_{CI(2)-(4)}$ are 0.81, 1.23, and 2.44 eV. As all these energy barriers are energy available for the 2-photon absorption experimental system, all four reaction channels are accessible. Another conical intersection $(S_1/S_0)_{CI(5)}$ is identified to which molecules can evolve from $S_{1,min}$ without a transition state: the energy barrier for this reaction path is 2.60 eV. The tetrazole ring at conical intersection $(S_1/S_0)_{CI(5)}$ does not open. As $(S_1/S_0)_{CI(5)}$ has the highest energy barrier compared to all the ring opening conical intersections, we suggest that the S_1 excited 5,5′-BT molecule is most likely to finish the ring opening process in the S_1 state, not ground state S_0. This mechanism is similar to that found for 1,5′-BT. The adiabatic energy gaps between S_1 and S_0 surfaces near $(S_1/S_0)_{CI(1)-(5)}$ are computed to be in the range between 13 and 132 cm^{-1}: the S_1 and S_0 surfaces are thereby strongly non-adiabatically coupled with one another and the small energy gaps increase

TABLE II. Summary of reaction paths and critical point energies for the 5,5′-BT decomposition reaction.

Reaction path	Color	$S_{1,TS}$	$S_{1,IM}$	$S_{1,TS2}$	$(S_1/S_0)_{CI}$	$S_{0,IM}$	$S_{0,TS}$	$S_{0,N2}$
(1)	Red	4.99	…	…	3.72	0.39	1.44	1.39
(2)	Orange	5.05	…	…	4.93	3.62	4.32	3.11
(3)	Pink	5.47	3.88	5.42	4.17	2.35	3.19	2.93
(4)	Green	6.68	…	…	5.67	3.29	3.85	2.39
(5)	Brown	…	…	…	6.84	0 (back to $S_{0,FC}$)	…	…

Details of each reaction path (i)

i = 1, 2, 4	$S_{min} \rightarrow S_{1,TS(i)} \rightarrow (S_1/S_0)_{CI(i)} \rightarrow S_{0,IM(i)} \rightarrow S_{0,TS(i)} \rightarrow S_{0,N2(i)}$
i = 3	$S_{min} \rightarrow S_{1,TS(3)} \rightarrow S_{1,IM} \rightarrow S_{1,TS2(3)} \rightarrow (S_1/S_0)_{CI(3)} \rightarrow S_{0,IM(3)} \rightarrow S_{0,TS(3)} \rightarrow S_{0,N2(3)}$
i = 5	$S_{min} \rightarrow (S_1/S_0)_{CI(5)} \rightarrow S_{0,FC}$

the probability of non-adiabatic transitions from upper to lower electronic states.

As the molecule moves from S_1 to S_0 state through $(S_1/S_0)_{CI(1)-(5)}$, the IRC algorithm shows that the steepest descent pathway for the molecule is to evolve either the stable intermediate state $S_{0,im(1)-(4)}$ or the Frank Condon structure $S_{0,FC}$. From the IRC scan, conical intersection $(S_1/S_0)_{CI(5)}$ leads back to the Franck-Condon structure. To undergo further decomposition reaction, the tetrazole ring should open: this reaction path does not generate 5,5′-BT decomposition. At intermediate states $S_{0,IM(1)-(4)}$, generated from $(S_1/S_0)_{CI(1)-(4)}$, the tetrazole ring remains open. From $S_{0,IM(1)-(4)}$, the molecule surmounts energy barriers in the range from 1.31 to 3.33 eV through the concerted transition states $S_{0,TS(1)-(4)}$ and forms N_2 products $S_{0,N2(1)-(4)}$. The N_2 products move away from the whole molecule without obvious torque for all the reaction channels shown in Figure 7. Therefore, N_2 products should have low rotational temperatures, as is consistent with the experimental results. The energies of the final product with dissociated N_2 in the four reaction paths are between 1.39 eV and 3.11 eV, implying that these N_2 products should have a high vibrational temperature.

5,5′-BT is electronically excited in the experiment and it absorbs two laser photons in addition its initial energy: it undergoes decomposition to form N_2 products, following four reaction paths as shown in Figure 7. Similar to 1,5′-BT, the tetrazole ring of 5,5′-BT opens on the first excited state S_1: the N_2 product is dissociated on the ground electronic state. The energy difference between the laser energy and the energy of the final structure with N_2 products with their internal energies is the energy released from 5,5′-BT decomposition in this initial molecular step. Based on the theoretical calculations, N_2 should have a high vibrational temperature. This conclusion is consistent with our previous studies of energetic materials, which find dissociated NO with a high vibrational temperature as the initial molecular decomposition step.[22,27,29–39]

Conical intersections are the key features in the excited electronic state chemistry of organic molecules in general, and energetic molecules in particular. 5,5′-BT has a similar structure to 1,5′-BT, with two attached tetrazole rings at carbon atom positions rather than at C–N positions (see Figure 1). Of the five conical intersections between S_0 and S_1 found for 5,5′-BT, four of them lead to decomposition to an N_2 product. The number of conical intersections found for 5,5′-BT between the S_1 and S_0 potential energy surfaces is lower than that found for 1,5′-BT because 5,5′-BT is a symmetric molecule and does not have as many different ring opening positions. Similar to 1,5′-BT, which ring position opens first is not important as the energy barriers for the tetrazole ring opening in different places are quite close (within 1.69 eV). Thus, both 1,5′-BT and 5,5′-BT are good energetic materials with numerous decomposition reaction channels and high explosive properties.

C. Calculations for AzTT

Schematic one-dimensional projections of the multi-dimensional singlet potential energy surfaces (S_0 and S_1) of AzTT, with locations and potential energies (the presented energies are not corrected for zero point energy) for different critical points and conical intersections along the minimum energy reaction paths, are plotted in Figure 9 and the energy for each point is summarized in Table III. Figure 9 describes eight different reaction mechanisms or channels for AzTT. The reaction coordinates depicted in Figure 9 include C–N and N–N bond lengths at the AzTT active sites. These sites include the tetrazole/triazole ring opening positions and breaking of the azide group. Arrows in Figure 9 indicate different possible reaction channels for AzTT decomposition. The structures of each critical point and conical intersection are summarized in Figure 10. In Figures 9 and 10, FC geometry $S_{0,FC}$ is the optimized minimum energy of AzTT on the S_0 state with a planar structure. $(S_1/S_0)_{CI(1)-(8)}$ are the conical intersections between the S_0 and S_1 states, and (1)-(8) related to different ring opening positions on the tetrazole/triazole rings, and rupture of the azide group in different reaction channels. $S_{1,TS(3)(4)(6)-(8)}$ are the excited transition states on the S_1 surface between the minimum structure $S_{1,min}$ and the related conical intersections. Some conical intersections do not have transition

TABLE III. Summary of reaction paths and critical point energies for the AzTT decomposition reaction.

Reaction path	Color	$S_{1,TS}$	$(S_1/S_0)_{CI}$	$S_{0,IM}$	$S_{0,TSa}$	$S_{0,N2a}$	$S_{0,TSb}$	$S_{0,N2b}$
(1)	Red	…	1.96	0 (back to $S_{0,FC}$)	1.09	0.07	…	…
(2)	Orange	…	5.07	0 (back to $S_{0,FC}$)	1.09	0.07	…	…
(3)	Pink	5.35	3.02	1.83	2.47	1.10	2.85	1.47
(4)	Green	5.44	1.77	0.13	…	1.07	0.83	0.07
(5)	Brown	…	5.64	3.53	4.39	2.13	3.82	0.60
(6)	Blue	5.73	4.23	−2.51	…	…	…	…
(7)	Purple	5.81	2.21	0.49	1.52	0.52	…	…
(8)	Black	6.49	5.06	1.26	2.24	1.60	2.74	1.17

Details of each reaction path (i)

i = 1, 2	$S_{min} \rightarrow (S_1/S_0)_{CI(i)} \rightarrow S_{0,FC} \rightarrow S_{0,TSa(i)} \rightarrow S_{0,N2a(i)}$
i = 3, 8	$S_{min} \rightarrow S_{1,TS(i)} \rightarrow (S_1/S_0)_{CI(i)} \rightarrow S_{0,IM(i)} \rightarrow S_{0,TSa(i)}$ (or $S_{0,TSb(i)}$) $\rightarrow S_{0,N2a(i)}$ (or $S_{0,N2b(i)}$)
i = 4	$S_{min} \rightarrow S_{1,TS(4)} \rightarrow (S_1/S_0)_{CI(4)} \rightarrow S_{0,IM(4)} \rightarrow S_{0,N2a(4)}$ (or $S_{0,TSb(4)} \rightarrow S_{0,N2b(4)}$)
i = 5	$S_{min} \rightarrow S_{1,TS(i)} \rightarrow (S_1/S_0)_{CI(5)} \rightarrow S_{0,IM(5)} \rightarrow S_{0,TSa(5)}$ (or $S_{0,TSb(5)}$) $\rightarrow S_{0,N2a(5)}$ (or $S_{0,N2b(5)}$)
i = 6	$S_{min} \rightarrow S_{1,TS(6)} \rightarrow (S_1/S_0)_{CI(6)} \rightarrow S_{0,IM(6)}$
i = 7	$S_{min} \rightarrow S_{1,TS(7)} \rightarrow (S_1/S_0)_{CI(7)} \rightarrow S_{0,IM(7)} \rightarrow S_{0,TSa(7)} \rightarrow S_{0,N2a(7)}$

states on the S_1 state; thus, $S_{1,TS}$ is not labeled from (1) to (8). $S_{0,IM(3)-(8)}$ are the intermediate states on S_0 after $(S_1/S_0)_{CI}$, and $S_{0,TSa(3)(5)(7)(8)}$ and $S_{0,TSb(3)(4)(5)(8)}$ are the transition states on the S_0 surface following the related intermediate states $S_{0,IM(3)-(8)}$ in different reaction channels. $S_{0,N2a(3)(4)(5)(7)(8)}$ and $S_{0,N2b(3)(4)(5)(8)}$ are N_2 dissociated products on the S_0 state.

The reaction paths in Figure 9 show that, with two photon absorption, AzTT can be excited to its S_n ($n > 8$) state and then evolve to the first excited electronic state S_1 through several conical intersections. On the S_1 state, AzTT undergoes a rapid internal conversion to the energy minimum structure $S_{1,min}$. Next, the molecule encounters energy barriers to transition states $S_{1,TS(3)(4)(6)-(8)}$ and passes to the ground electronic state through the $(S_1/S_0)_{CI(1)-(8)}$ conical intersections: molecules undergoing this process would place sufficient vibrational energy in the S_0 state, transferred from the S_n electronic energy, to dissociate. The five transition states on the S_1 PES are related to five different tetrazole/triazole ring opening conical intersections. The energies of these transition states are listed in Table III: energy barriers from $S_{1,imn}$ to the transition states are between 3.61 eV and 4.75 eV. Among these five reaction channels, the reaction path with the lowest transition state energy is shown in Figure 9 in violet (reaction path (3) in Figure 9 and Table III). On the violet (3) path, the molecule moves from $S_{1,min}$, surmounts a 3.61 eV energy barrier to $S_{1,TS(3)}$ and then reaches conical intersection $(S_1/S_0)_{CI(3)}$ at which the tetrazole ring opens at bond N2′–N3′. Another three conical intersections $(S_1/S_0)_{CI(1)}$, $(S_1/S_0)_{CI(2)}$, and $(S_1/S_0)_{CI(5)}$ are identified: the path to the latter conical intersection ($(S_1/S_0)_{CI(5)}$) has no transition states from $S_{1,min}$. The energy barriers for these three conical intersections are 0.22, 3.33, and 3.90 eV, respectively. $(S_1/S_0)_{CI(1)}$ and $(S_1/S_0)_{CI(2)}$ are the conical intersections between S_0 and S_1 states without tetrazole/triazole ring opening. At $(S_1/S_0)_{CI(5)}$, the triazole ring opens at N3—C2. The structure of $(S_1/S_0)_{CI(1)}$ is close to that of $S_{1,min}$: the energy barrier along this path is much lower than that for the other seven reaction paths. Thus, the most probable reaction path producing N_2 from AzTT is the red path (reaction path (1) in Figure 9 and Table III). Unlike 1,5′-BT and 5,5′-BT molecules opening the tetrazole ring on the S_1 state and producing N_2 following the ring opening on the ground state S_0, the tetrazole/triazole ring of AzTT most likely stays closed from high electronic states to ground state. The adiabatic energy gaps between the S_1 and S_0 surfaces near $(S_1/S_0)_{CI(1)-(8)}$ are computed to be in the range between 13 and 176 cm^{-1}; therefore, the S_1 and S_0 surfaces are strongly non-adiabatically coupled with one another and the small energy gap increases the probability of non-adiabatic transition from upper to lower electronic states.

As the molecule transitions from the S_1 to S_0 state through $(S_1/S_0)_{CI(1)-(8)}$, the IRC algorithm shows that the steepest descent pathway for the molecule is to evolve to either the stable intermediate state $S_{0,im(3)-(8)}$ or the Frank-Condon structure $S_{0,FC}$. Based on the IRC scan, conical intersections $(S_1/S_0)_{CI(1)}$ and $(S_1/S_0)_{CI(2)}$ return to the Frank-Condon structure. To produce N_2 product, as shown for the red path in Figure 9 (reaction path (1)), the N–N bond of the azide group breaks with an energy barrier of 1.09 eV through the transition state $S_{0,TSa(1)(2)}$. On this reaction path, the energy of the final molecule $S_{0,N2a(1)(2)}$ with N_2 product dissociated from azide group is 0.06 eV. Along other reaction paths, the tetrazole/triazole ring of intermediate states $S_{0,IM(3)(4)(8)}$ from $(S_1/S_0)_{CI(3)(4)(8)}$ stays open (reaction paths violet (3), green (4), and black (8) in Figure 9 and Table III). From $S_{0,IM(3)(4)(8)}$, N_2 can be created in two way: from the opened tetrazole/triazole ring or from azide group. As shown in Figure 9, reaction paths (3), (4), and (8) have two different channels after $S_{0,IM(3)(4)(8)}$, which are related to the two N_2 generation channels: (1) from $S_{0,TSa}$ to $S_{0,N2a}$; and (2) from $S_{0,TSb}$ to $S_{0,N2b}$.

After the IRC scan of $(S_1/S_0)_{CI(7)}$, the tetrazole ring of AzTT is closed; however, the molecular structure is not the same as that at $S_{0,FC}$. In this case, N_2 can only be formed from the azide group as shown in purple in Figure 9 (reaction path (7) in Figure 9 and Table III). From the IRC scan of $(S_1/S_0)_{CI(6)}$, N_2 product is already produced at $S_{0,IM(6)}$ from the opened triazole ring; therefore, no further research is explored in this case (blue path (6) in Figure 9 and Table III). N_2 products move away from the remaining molecule without obvious torque for all the reaction channels shown in Figure 9. Therefore, N_2 products should have low rotational temperatures, as is consistent with the experimental results. Energies of the final products with dissociated N_2 for the eight reaction paths are in the range of −2.51 eV and 2.13 eV. The energy difference between the laser energy, which is the original molecule energy, and the energy of the final structure with N_2 products and their internal energies, is the energy released from AzTT decomposition in its initial decomposition step. Based on the theoretical calculation, N_2 should have a high vibrational temperature.

The reaction mechanisms for AzTT underscore the importance of the azide group for energetic materials. Because 1,5′-BT and 5,5′-BT do not contain an azide group, their decomposition has to be initiated from the opening of tetrazole rings. Although the AzTT molecule can also decompose through tetrazole/triazole ring openings, the energy barrier for AzTT generating N_2 from the azide group without tetrazole/triazole ring opening is about 3 eV lower than those for ring opening. With the azide group, the decomposition of AzTT is much less energy intensive compared to the decomposition of 1,5′-BT and 5,5′-BT. The azide group in nitrogen rich energetic materials replaces the nitramine or NO_2 group of the older energetic molecules, which is the active site for the initial stages of the decomposition reaction in those systems.

From our previous studies on energetic materials, the NO product from energetic materials usually has a cold rotational temperature and a hot vibrational temperature.[22,27,29–39] The N_2 product observed from energetic salts TKX-50 and MAD-X1 has low rotational temperature and high theoretical vibrational temperature.[29] The behavior of the N_2 product from 1,5′-BT, 5,5′-BT, and AzTT is consistent with the behavior of the previous energetic materials reported.[22,27,29–39] The vibrational temperature of the initial dissociation product is important in recognizing energetic molecules because initial decomposition products with high vibrational excitation are better able to propagate a chain reaction following the initial stimulus, leading to detonation. With vibrationally hot N_2 as an initial dissociation products, the energetic properties of

1,5′-BT, 5,5′-BT, and AzTT are similar as the older energetic materials. The $S_n \rightarrow \cdots \rightarrow S_o$ pathway through a series of conical intersections leaves the molecule on a new part of the S_0 potential energy surface, not necessary near the FC equilibrium point.[33,34] Thereby, all the excitation energies are available to break internal bonds to generate reactive fragments and radicals for further reactions as may be required to be classified as a high energy molecule as an energetic material.

VI. CONCLUSIONS

Decomposition of the nitrogen rich energetic materials 1,5′-BT, 5,5′-BT, and AzTT following electronic excitation has been explored via nanosecond, energy resolved spectroscopy. These materials create N_2 as initial decomposition products through a number of distinct reaction channels. The rotational temperature of N_2 products from all three nitrogen rich energetic materials is cold (<30 K). Based on the experimental observations and CASSCF theoretical calculations, we conclude that N_2 products are released by the opening of tetrazole ring of 1,5′-BT and 5,5′-BT. The tetrazole ring opens on the S_1 excited state and N_2 product is formed on the ground state. For the AzTT molecule, N_2 is created by N–N bond breaking of the azide group on the S_0 state: this process has a much lower energy barrier than tetrazole/triazole ring opening decomposition mechanisms. The vibrational temperatures of N_2 product from all three energetic materials are hot based on theoretical calculation. Conical intersections are the key point for the theoretically derived mechanisms, as they provide non-adiabatic radiationless internal conversion between upper and lower electronic states on the fs time scale and place the undissociated molecule on a new part of the ground state potential surface with all its excitation energy in the ground state vibrations available for bond breaking.

ACKNOWLEDGMENTS

This study is supported by a grant from the U.S. Army Research Office (No. ARO, FA9550-10-1-0454 and W911-NF13-10192) and in part by the U.S. National Science Foundation (NSF) through the XSEDE supercomputer resources provided by NCSA under Grant No. TG-CHE110083. We also want to thank Professor Dr. Thomas M. Klapötke, Ludwig-Maximilian University of Munich for supplying the 5,5′-Bistetrazole, 1,5′-Bistetrazole and Azidotriazolyl-tetrazole samples used in this study and for helpful advice on their properties and handling.

[1]X.-H. Ju, H.-M. Xiao, and Q.-Y. Xia, "A density functional theory investigation of 1,1-diamino-2,2-dinitroethylene dimers and crystal," J. Chem. Phys. **119**, 10247 (2003).
[2]B. M. Rice, S. Sahu, and F. J. Ownes, "Density functional calculations of bond dissociation energies for NO_2 scission in some nitroaromatic molecules," J. Mol. Struct. (Theochem) **583**, 69 (2002).
[3]L. Turker and S. Varis, "Effects of epoxidation and nitration on ballistic properties of FOX-7 – A DFT study," Z. Anorg. Allg. Chem. **639**, 982 (2013).
[4]W. Zhu, C. Zhang, T. Wei, and H. Xiao, "Computational study of energetic nitrogen-rich derivatives of 1,1′- and 5,5′-bridged ditetrazoles," J. Comput. Chem. **32**, 2298 (2011).
[5]N. Fischer, D. Izsak, T. M. Klapotke, S. Rappengluck, and J. Stierstorfer, "Nitrogen-rich 5,5′-bistetrazolates and their potential use in propellant systems: A comprehensive study," Chem. - Eur. J. **18**, 4051 (2012).
[6]S. Huber, D. Izsak, K. Karaghiosoff, T. M. Klapotke, and S. Reuter, "Energetic salts of 5-(5-Azido-1H-1,2,4-triazol-3-yl)tetrazole," Propellants, Explos., Pyrotech. **39**, 793 (2010).
[7]N. Fischer, D. Izsak, T. M. Klapotke, and J. Stierstorfer, "The chemistry of 5-(Tetrazol-1-yl)-2H-tetrazole: An extensive study of structural and energetic properties," Chem. - Eur. J. **19**, 9848 (2013).
[8]S. Lobbecke, A. Pfeil, H. H. Krause, J. Sauer, and U. Holland, "Thermoanalytical screening of nitrogen-rich substances," Propellants, Explos., Pyrotech. **24**, 168 (1999).
[9]P. J. Eulgem, A. Klein, N. Maggiarosa, D. Naumann, and R. W. H. Pohl, "New rare earth metal complexes with nitrogen-rich ligands: 5,5′-bitetrazolate and 1,3-Bis(tetrazol-5-yl)triazenate—On the borderline between coordination and the formation of salt-like compounds," Chem. - Eur. J. **14**, 3727 (2008).
[10]L. H. Finger, F. G. Schroder, and J. Sundermeyer, "Synthesis and characterisation of 5,5′-bistetrazolate salts with alkali metal, ammonium and imidazolium cations," Z. Anorg. Allg. Chem. **639**, 1140 (2013).
[11]N. Fischer, T. M. Klapotke, K. Peters, M. Rusan, and J. Stierstorfer, "Alkaline earth metal salts of 5,5_-Bistetrazole—From academical interest to practical application," Z. Anorg. Allg. Chem. **637**, 1693 (2011).
[12]A. A. Dippold and K. M. Klapotke, "Synthesis and characterization of 5-(1,2,4-triazol-3-yl)tetrazoles with various energetic functionalities," Chem. Asian. J. **8**, 1463 (2013).
[13]B. Tan, X. Long, R. Peng, H. Li, B. Jin, S. Chu, and H. Dong, "Two important factors influencing shock sensitivity of nitro compounds: Bond dissociation energy of X–NO_2 (X = C, N, O) and mulliken charges of nitro group," J. Hazard. Mater. **183**, 908 (2010).
[14]M. R. Manaa, L. E. Fried, C. F. Melius, M. Elstner, and Th. Frauenheim, "Decomposition of HMX at extreme conditions: A molecular dynamics simulation," J. Phys. Chem. A **106**, 9024 (2002).
[15]C. Ye and J. M. Shreeve, "New Atom/Group volume additivity method to compensate for the impact of strong hydrogen bonding on densities of energetic materials," J. Chem. Eng. Data **53**, 520 (2008).
[16]G. F. Adams and R. W. Shaw, Jr., "Chemical reactions in energetic materials," Annu. Rev. Phys. Chem. **43**, 311 (1992).
[17]R. Behrens, Jr., "Thermal decomposition of energetic materials: Temporal behaviors of the rates of formation of the gaseous pyrolysis products from condensed-phase decomposition of octahydro-1,3,5,7-tetranitro-1,3,5,7-tetrazocine," J. Phys. Chem. **94**, 6706 (1990).
[18]D. Furman, R. Kosloff, F. Dubnikova, S. V. Zybin, W. A. Goddard III, N. Rom, B. Hirshberg, and Y. Zeiri, "Decomposition of condensed phase energetic materials: Interplay between uni- and bimolecular mechanisms," J. Am. Chem. Soc. **136**, 4192 (2014).
[19]A. Bhattacharya, Y. Q. Guo, and E. R. Bernstein, "Nonadiabatic reactions of energetic molecules," Acc. Chem. Res. **43**, 1476 (2010).
[20]M. M. Kuklja, "Role of electronic excitations in explosive decomposition of solids," J. Appl. Phys. **89**, 4156 (2001).
[21]E. J. Reed, J. D. Joannopoulos, and L. E. Fried, "Electronic excitations in shocked nitromethane," Phys. Rev. B. **62**, 16500 (2000).
[22]Y. Q. Guo, A. Bhattacharya, and E. R. Bernstein, "Decomposition of nitramine energetic materials in excited electronic states: RDX and HMX," J. Chem. Phys. **122**, 244310 (2005).
[23]Y. Q. Guo, M. Greenfield, A. Bhattacharya, and E. R. Bernstein, "On the excited electronic state dissociation of nitramine energetic materials and model systems," J. Chem. Phys. **127**, 154301 (2007).
[24]K. L. Carleton, K. H. Welge, and S. R. Leone, "Detection of nitrogen rotational distributions by resonant 2 + 2 multiphoton ionization through the $a^1\Pi_g$ state," Chem. Phys. Lett. **115**, 492 (1985).
[25]G. O. Sitz, A. C. Kummel, and R. N. Zare, "Population and alignment of N_2 scattered from Ag(111)," J. Vac. Sci. Technol., A **5**, 513 (1987).
[26]F. J. Aoiz, L. Banares, V. J. Herrero, B. Martinez-Haya, M. Menendez, P. Quintana, L. Tanarro, and E. Verdasco, "Low-temperature rotational relaxation of N_2 in collisions with Ne," J. phys. Chem. A. **105**, 6976 (2001).
[27]A. Bhattacharya and E. R. Bernstein, "Nonadiabatic decomposition of Gas-Phase RDX through conical intersections: An ONIOM-CASSCF study," J. Phys. Chem. A **115**, 4135 (2011).

[28]H. Mori, T. Ishida, Y. Aoki, and T. Niimi, "Spectroscopic study of REMPI for rotational temperature measurement in highly rarefied Gas," AIP Conf. Proc. **585**, 956 (2001).
[29]B. Yuan, Z. Yu, and E. R. Bernstein, "Initial mechanisms for the decomposition of electronically excited energetic salts: TKX-50 and MAD-x1," J. Phys. Chem. A (published online).
[30]A. Bhattacharya, Y. Q. Guo, and E. R. Bernstein, "Unimolecular decomposition of tetrazine-N-oxide based high nitrogen content energetic materials from excited electronic states," J. Chem. Phys. **131**, 194304 (2009).
[31]A. Bhattacharya, Y. Q. Guo, and E. R. Bernstein, "Experimental and theoretical exploration of the initial steps in the decomposition of a model nitramine energetic material: Dimethylnitramine," J. Phys. Chem. A **113**, 811 (2009).
[32]Z. Yu and E. R. Bernstein, "Decomposition of pentaerythritoltetranitrate [$C(CH_2ONO_2)_4$] following electronic excitation," J. Chem. Phys. **135**, 154305 (2011).
[33]Z. Yu and E. R. Bernstein, "Experimental and theoretical studies of the decomposition of new imidazole based energetic materials: Model systems," J. Chem. Phys. **137**, 114303 (2012).
[34]Z. Yu and E. R. Bernstein, "On the decomposition mechanisms of new imidazole-based energetic materials," J. Phys. Chem. **117**, 1756 (2013).
[35]Y. Q. Guo, A. Bhattacharya, and E. R. Bernstein, "Decomposition of excited electronic state s-tetrazine and its energetic derivatives," J. Chem. Phys. **134**, 024318 (2011).
[36]Y. Q. Guo, A. Bhattacharya, and E. R. Bernstein, "Excited electronic state decomposition of furazan based energetic materials: 3,3′-Diamino-4,4′-azoxyfurazan and its model systems, diaminofurazan and furazan," J. Chem. Phys. **128**, 034303 (2008).
[37]Y. Q. Guo, A. Bhattacharya, and E. R. Bernstein, "Ultrafast S_1 to S_0 internal conversion dynamics for dimethylnitramine through a conical intersection," J. Phys. Chem. A **115**, 9349 (2011).
[38]B. Yuan, Z. Yu, and E. R. Bernstein, "Azole energetic materials: Initial mechanisms for the energy release from electronical excited nitropyrazoles," J. Chem. Phys. **140**, 034320 (2014).
[39]B. Yuan, Z. Yu, and E. R. Bernstein, "Initial decomposition mechanism for the energy release from electronically excited energetic materials: FOX-7 (1,1-diamino-2,2-dinitroethene, $C_2H_4N_4O_4$)," J. Chem. Phys. **140**, 074708 (2014).